

## Estimation of the diffuse attenuation coefficient $K_{dPAR}$ using MERIS and application to seabed habitat mapping

Bertrand Saulquin<sup>a,\*</sup>, Anouar Hamdi<sup>b</sup>, Francis Gohin<sup>c</sup>, Jacques Populus<sup>c</sup>, Antoine Mangin<sup>a</sup>,  
Odile Fanton d'Andon<sup>a</sup>

<sup>a</sup> ACRI-ST, Sophia-Antipolis, France

<sup>b</sup> Institut des Milieux Aquatiques, Bayonne, France

<sup>c</sup> Ifremer, Brest, France

\*: Corresponding author : Bertrand Saulquin, Tel.: + 33 492967128 ; email address : [bertrand.saulquin@acri-st.fr](mailto:bertrand.saulquin@acri-st.fr)

### Abstract:

The availability of light in the water column and at the seabed determines the euphotic zone and constrains the type and the vertical distribution of algae species. Light attenuation is traditionally quantified as the diffuse attenuation coefficient of the downwelling spectral irradiance at wavelength 490 nm ( $K_{d490}$ ) or the photosynthetically available radiation ( $K_{dPAR}$ ). Satellite observations provide global coverage of these parameters at high spatial and temporal resolution and several empirical and semi-analytical models are commonly used to derive  $K_{d490}$  and  $K_{dPAR}$  maps from ocean colour satellite sensors. Most of these existing empirical or semi-analytical models have been calibrated in open ocean waters and perform well in these regions, but tend to underestimate the attenuation of light in coastal waters, where the backscattering caused by the suspended matters and the absorption by the dissolved organic matters increase light attenuation in the water column.

We investigate two relationships between  $K_{dPAR}$  and  $K_{d490}$  for clear and turbid waters using MERIS reflectances and the spectral diffuse attenuation coefficient  $K_d(\lambda)$  developed by Lee (2005). Satellite-derived fields of  $K_{d490}$  and modelled  $K_{dPAR}$  are evaluated using coincident in-situ data collected over the world in both clear and turbid waters, and by using Ecolight simulations. Temporal means at 250 m resolution of  $K_{dPAR}$  and euphotic depth were computed over the period 2005–2009 for European coastal waters. These mean data were cross-tabulated with in-situ data of kelp (*Laminaria hyperborea*) and seagrass (*Posidonia oceanica*), respectively observed at locations on Atlantic and Mediterranean shores where the light is taken as the limiting factor to the depth distribution for these species. The minima observed for *P. oceanica*, in percent of energy, are very close to 1% of surface irradiance, the historical threshold known as euphotic depth as defined by Ryther (1956). Real estimates of the surface irradiance (Frouin, 1989) are used in conjunction with the estimated  $K_{dPAR}$  to calculate the residual energy at the lower limit of *P. oceanica* and *L. hyperborea* in  $\text{mol}\cdot\text{photons}\cdot\text{m}^{-2}\cdot\text{day}^{-1}$  as a complement to the usual fraction of the surface energy. We show that the observed values, in terms of energy, for both species were equivalent to the values reported in the literature.

### Highlights

► We compare the most common models of satellite derived  $K_{d490}$  to an in-situ dataset. ► We propose two relationships between the mean  $K_{dPAR}$  and the  $K_{d490}$ . ► We generate high resolution maps of  $K_{dPAR}$  and  $Z_{EU}$  over Europe. ► These maps are cross-tabulated with in-situ coverage of kelp and seagrass. ► The observed minimum for light, in percent and energy, is compared to the literature.

**Keywords:** Ocean color ; Light attenuation ; Photosynthetic available radiation ; Euphotic depth ; Seabed mapping

### 1. Introduction

The light available in the water column at wavelengths between 400 and 700 nm in the

48 visible part of the spectrum, termed photo-synthetically active radiation (PAR), is utilised by  
49 phytoplankton for photosynthesis (Kirk, 1994; Falkowski *et al.*, 1997) and constrains the  
50 type and distribution of algae species and benthic algae which can contribute significantly  
51 to total primary production (Cahoon *et al.*, 1993; McMinn *et al.*, 2005). The estimation of  
52 the light attenuation in the water column is also critical to understand physical processes  
53 such as the heat transfer in the upper layer of the ocean (Lewis *et al.*, 1990; Morel *et al.*,  
54 1994; Sathyendranath *et al.*, 1991; Wu *et al.*, 2007). From an optical perspective, in  
55 addition to pure water, light attenuation is constrained by the concentration of three  
56 components (IOCCG Report 3, 2000): pigments, expressed here as the concentration of  
57 chlorophyll-a ([Chl-a]), dissolved yellow substances (gelbstoff or CDOM) absorption  $a_{\text{cdm}}$   
58 and suspended particulate matter concentration ([SPM]). In-situ spectral diffuse  
59 attenuation coefficient  $K_d(\lambda)$  was traditionally measured by the ocean-colour scientific  
60 community at 490 nm ( $K_{d490}$ ), following the first studies in the 1970's (Jerlov, 1976).  
61 Concurrently, biologists have focused on the PAR measurement and attenuation ( $K_{d\text{PAR}}$ ).  
62 Both  $K_{d\text{PAR}}$  and  $K_{d490}$  increase with increasing solar zenith angle and  $K_{d\text{PAR}}$  is significantly  
63 depth dependent (the longer wavelength, here the red, is more quickly attenuated in the  
64 water column than the shorter one, here the blue ) even for well-mixed waters.

65

66 Since the launch of the Coastal Zone Color Scanner (CZCS) in 1978, the ocean-colour  
67 community has provided maps of  $K_{d490}$  or  $K_{d\text{PAR}}$  at large scales offering a great increase of  
68 spatial and temporal measurements compared to *in-situ* data. Space based sensors  
69 measure top-of-atmosphere radiances at different wavelengths and the Medium  
70 Resolution Imaging Spectrometer (MERIS) sensor has 15 bands between 412 and 865  
71 nm. The contribution from the atmosphere is firstly removed from the top-of-atmosphere  
72 radiance, through a process known as atmospheric correction (Gordon *et al.*,1994), to

73 obtain the water-leaving radiance ( $L_w$ ). The  $L_w$  are normalised, i.e. expressed in standard  
74 solar conditions (sun at zenith), in the absence of the atmosphere, and corrected for  
75 bidirectional effects (viewing angle dependence and effects of seawater anisotropy, Morel  
76 *et al.*, 2002) to obtain the normalised water-leaving radiance ( $nL_w$ ). Today, several  
77 empirical and semi-analytical models of  $K_{d490}$  and  $K_{dPAR}$  are commonly used to derive  $K_{d490}$   
78 maps from satellite-derived  $nL_w$ .

79 Mueller (2000) defines an empirical relationship between  $K_{d490}$  and the ratio between  
80 blue and green water-leaving radiances from the Sea-viewing Wide Field-of-view Sensor  
81 (SeaWiFS) (McClain *et al.*, 2004), and the Moderate Resolution Imaging  
82 Spectroradiometer (MODIS) (Esaias *et al.*, 1998). Morel (2007) proposes an empirical  
83 relationship between the  $K_{d490}$  and the Chl-a concentration. Lee (2002, 2005a, 2005b,  
84 2007) provided a semi-analytical for  $K_{d490}$  with dedicated versions for SeaWiFS, MERIS  
85 and MODIS  $nL_w$ .

86

87  $K_{dPAR}$  was historically expressed as a function of [Chl-a] (Morel, 1988) for clear waters.  
88 This latest approach is routinely used in the open ocean where phytoplankton is the main  
89 contributor to attenuation (Claustre *et al.*, 2003), but its use is, however, not  
90 straightforward in the coastal ocean where light attenuation by CDOM and SPM may be  
91 significant (Case 2 waters). In coastal areas regional approaches express  $K_{dPAR}$  as a  
92 function of the [Chl-a], and [SPM] (Gohin *et al.*, 2005; Delvin *et al.*, 2009). Recently,  $K_{dPAR}$   
93 is more often related to  $K_{d490}$  using empirical approaches and the relationship between  
94  $K_{d490}$  and  $K_{dPAR}$  has quite large regional variations (Zaneveld *et al.*, 1993; Barnard *et al.*,  
95 1999; Morel *et al.*, 2007; Pierson *et al.*, 2008; Kratzer, 2008; Wang, 2009).

96

97 In this paper, we briefly show the performance of three models of  $K_{d490}$  (Mueller, 2000;

98 Morel *et al.*, 2007; Lee *et al.*, 2005), routinely used in the standard MERIS, SeaWiFS and  
99 MODIS Level 3 products, compared to an *in-situ* dataset collected near shore and in clear  
100 open sea waters. We then derive two relationships between  $K_{dPAR}$  and  $K_{d490}$ , estimated by  
101 integrating the spectral irradiances over the euphotic depth and the visible spectrum using  
102  $K_d(\lambda)$  as estimated by Lee *et al.* (2005).

103

104 Our aim is to provide an estimation of  $K_{dPAR}$  for values greater than  $0.06 \text{ m}^{-1}$  and lower  
105 than  $1 \text{ m}^{-1}$ . For more turbid waters, dedicated algorithms may be used, and for oligotrophic  
106 waters ( $K_{dPAR} < 0.06 \text{ m}^{-1}$ ), standard  $K_{dPAR}$  estimations (Morel *et al.*, 2007, Mueller *et al.*,  
107 2000) are freely available at 4 km resolution on the Globcolour webpage  
108 [www.globcolour.info](http://www.globcolour.info), and the oceancolor webpage <http://oceancolor.gsfc.nasa.gov/>.

109

110 In a second step, temporal means of satellite derived  $K_{dPAR}$  and Zeu were calculated  
111 over Europe from 2005 to 2009 to characterise a reference state for light and marine  
112 coastal fauna and flora from intertidal area to Zeu at 250m resolution.

113

114 In a last step, six sites were selected by Ifremer in Corsica (Mediterranean Sea) and  
115 in Brittany (English Channel and Atlantic Ocean) to compare the satellite derived minimum  
116 light threshold values for *P. oceanica* and *L. hyperborea* to the literature. The threshold of  
117 1% used to define Zeu as the minimum light requirement for benthic primary production,  
118 was historically determined from *in-situ* observations of *P. oceanica* in the Mediterranean  
119 Sea. We therefore compare the satellite-derived 1% to the deepest depth at which *P.*  
120 *oceanica* is observed in the Corsica. Nevertheless, some species can survive at lower light  
121 levels and the evaluation of the light available in fraction of the surface irradiance is  
122 biologically meaningless (Gattuso, 2006) as the fraction of moonlight is the same than the

123 fraction of sunlight. Therefore, we propose in this section the use of daily integrated PAR  
124 (Frouin, 1998), attenuated into the water column using  $K_{dPAR}$ , to arrive at an estimation of  
125 the PAR in the water column in  $\text{mol.photons.m}^{-2}.\text{d}^{-1}$ , a more meaningful estimation of  
126 energy in the water column than fraction of the surface energy, generally used by the  
127 community.

128

## 129 **II. Methods**

130

131 The spectral diffuse attenuation coefficient  $K_d(\lambda)$  is the coefficient of the exponential  
132 attenuation of the spectral downwelling irradiance:

133

$$134 \quad E_d(\lambda) = E_0(\lambda).e^{-K_d(\lambda)z} \quad (1)$$

135

136 Here  $E_d(\lambda)$  is the spectral downwelling irradiance in  $\text{W.m}^{-2}.\text{nm}^{-1}$  at depth  $z$  and  
137 wavelength  $\lambda$  ( $E_0(\lambda)$  is the energy just beneath the surface). If the visible spectral domain  
138 is considered, the PAR at depth  $z$  can be related to  $K_d(\lambda)$  and  $E_d(\lambda)$  using energetic (Eq  
139 2a) or quantum units (Eq. 2b.) (Baker *et al.*, 1987; Morel *et al.*, 1974):

140

$$141 \quad PAR(z) = \int_{400nm}^{700nm} E_d(\lambda; z=0). \exp^{-K_d(\lambda).z} d\lambda \quad [\text{W.m}^{-2}] \quad (2a)$$

142 
$$PAR(z) = \frac{1}{h.c} \int_{400nm}^{700nm} \lambda \cdot E_d(\lambda; z=0) \cdot \exp^{-K_d(\lambda) \cdot z} d\lambda \quad [\text{photons} \cdot \text{m}^{-2} \cdot \text{s}^{-1}] \quad (2b)$$

143 An expression of the instantaneous  $K_{dPAR}(z)$  is:

144

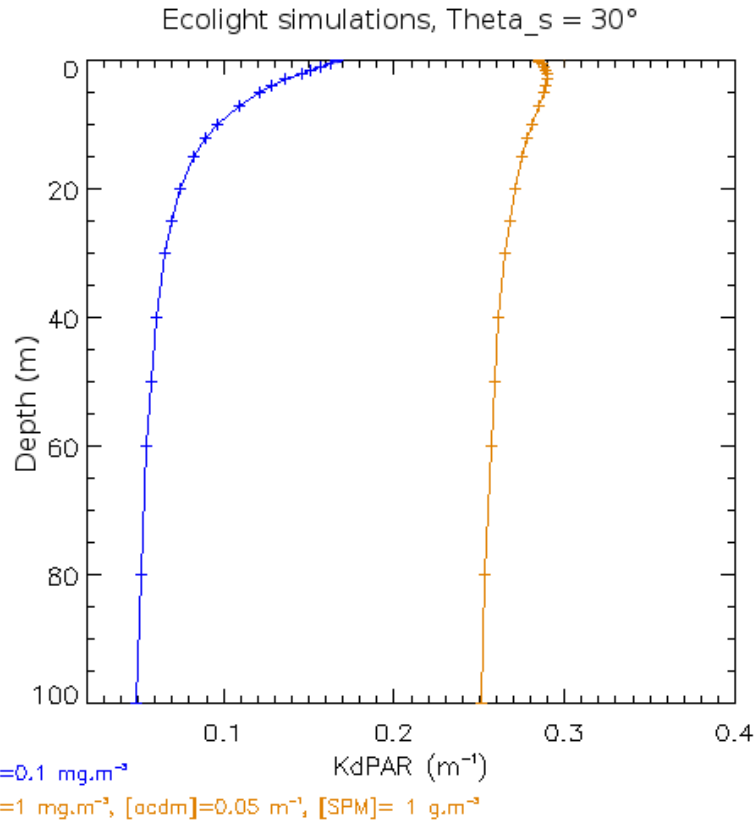
145 
$$K_{dPAR}(z) = -\frac{\ln(PAR(z+dz)) - \ln(PAR(z))}{dz} \quad (3)$$

146

147  $K_{dPAR}$  changes with depth as the red photons are absorbed in the top layers. The  
 148 spectral diffuse attenuation coefficient of downwelling irradiance  $K_d(\lambda)$  also changes with  
 149 depth, but its magnitude of variation is significantly smaller than that of  $K_{dPAR}$  (Lee, 2009;  
 150 Zaneveld *et al.*, 1993). The Hydrolight / Ecolight (© Curtis D. Mobley, 2008) is a radiative  
 151 transfer model that computes radiance distributions and related quantities (irradiance,  
 152 reflectances, diffuse attenuation functions, etc ...) in any water body starting from the Chl-a  
 153 and SPM concentration and CDOM absorption. Figure 1 shows two Ecolight simulations  
 154 of  $K_{dPAR}$  for clear (blue) and coastal turbid water (orange). In this simulation the water is  
 155 assumed to be well mixed with a [Chl-a] of  $0.1 \text{ mg} \cdot \text{m}^{-3}$  (blue line) and scattering of  
 156 particulates is based on the model of Gordon and Morel (1983). The sky is assumed  
 157 cloudless with the sun at  $30^\circ$  from the zenith. For coastal water simulation (orange), [Chl-a]  
 158 is set to  $1 \text{ mg} \cdot \text{m}^{-3}$ ,  $a_{cdom}$  to  $0.05 \text{ m}^{-1}$  and [SPM] to  $1 \text{ g} \cdot \text{m}^{-3}$ . The instantaneous  $K_{dPAR}$  (Figure  
 159 1) is estimated using Eq 3. Figure 1 verifies that  $K_{dPAR}(z)$  is more constant for coastal  
 160 turbid waters (Wang, 2009).

161

162



163

164

Figure 1: Simulated  $K_{dPAR}(z)$  in the water column using Ecolight for clear water with low [Chl-a] (case1, blue) and coastal water (case 2, orange).

165

166

167

We consider in this paper the vertical average value of  $K_{dPAR}$  between the surface and

168

the euphotic depth,  $\overline{K_{dPAR}}$  (Eq. 5) because  $K_{dPAR}$  values reported in the literature or *in-*

169

*situ* databases used for validation are based on this expression.

170

171

$$\overline{KdPAR} = \frac{\ln(PAR(0)) - \ln(PAR(z))}{z} \quad (4)$$

172

We use  $z = Z_{eu}$  in this study. Using  $\overline{K_{dPAR}}$ , instead of  $K_{dPAR}(z)$  will lead to an accurate

173

estimation of PAR near the surface and  $Z_{eu}$ . Between these two depths, PAR will be

174

slightly over-estimated. Further in this paper,  $\overline{K_{dPAR}}$  is noted  $K_{dPAR}$ .

175

Table 1: list of symbols

Symbol	Definition	Unit
L <sub>w</sub>	Water leaving radiance	W.m <sup>-2</sup> .sr <sup>-1</sup> .m <sup>-1</sup>
a(λ)	absorption coefficient at wavelength λ	m <sup>-1</sup>
bb(λ)	backscattering coefficient at wavelength λ	m <sup>-1</sup>
CDOM	Coloured Dissolved organic matters	
Chl-a	Chlorophyll-a	
DTM	Digital Terrain Model	
GSM	Garver-Siegel-Maritorena	
Globcolour	Global Ocean Colour ESA funded project	
SPM	Suspended particulate matter	
E <sub>d</sub> (λ, z)	Spectral downwelling irradiance at depth z	W.m <sup>-2</sup> .m <sup>-1</sup>
IOP	Inherent Optical Properties	
K <sub>d</sub> (λ, E%)	Spectral diffuse attenuation coefficient for downwelling irradiance between E <sub>d</sub> (λ,0) and % of E <sub>d</sub> (λ,0)	m <sup>-1</sup>
K <sub>dPAR</sub>	Diffuse attenuation coefficient of PAR	m <sup>-1</sup>
$\overline{K_{dPAR}}$	Vertical average value of mean diffuse attenuation coefficient over the euphotic layer	m <sup>-1</sup>

MERIS	Medium Resolution Imaging Spectrometer	
MODIS	Moderate Resolution Imaging Spectroradiometer	
PAR	Photosynthetically Available Radiation	photons.m <sup>-2</sup> .s <sup>-1</sup> or W.m <sup>-2</sup>
Rrs	Remote sensing reflectance (ratio of water-leaving radiance to downwelling irradiance above the surface)	
SHOM	Service Hydrographique et Océanographique de la Marine	
SeaWiFS	Sea-viewing Wide Field-of-view Sensor	
Zeu	Euphotic depth	m
Z <sub>490</sub>	Depth at which E(Z,490)=1%E(0,490)	m
Z <sub>90</sub>	First optical layer =1./ K <sub>d490</sub>	m
Θ <sub>s</sub> , Theta_s	above surface solar zenith angle	Radians

178

### 179 **III. In Situ Data**

#### 180 **A. K<sub>d490</sub>, K<sub>dPAR</sub> measurements**

181 *In-situ* Ed(λ,z) or PAR(z) measurements must be collected following a community-  
 182 vetted protocol, (Werdell *et al*, 2005) to avoid ship shadow and reflectance. If required (not  
 183 here), PAR irradiance data expressed in W.m<sup>-2</sup> can be converted to molar units using the

184 following approximation:  $2.5 \times 10^{18}$  quanta  $s^{-1} \cdot W^{-1}$  or  $4.2 \mu E \cdot m^{-2} \cdot s^{-1} \cdot W^{-1}$  (Morel *et al*,  
185 1974). In-situ data of  $K_{d490}$  and  $K_{dPAR}$  available through global datasets such as NOMAD  
186 [http://seabass.gsfc.nasa.gov/data/nomad\\_seabass\\_v2.a\\_2008200.txt](http://seabass.gsfc.nasa.gov/data/nomad_seabass_v2.a_2008200.txt),

187 SeaBASS (<http://seabass.gsfc.nasa.gov/>) were extracted over the period 2005 to  
188 2009.

189  
190 Data from the instrumented buoy BOUSSOLE located near Villefranche (France) in  
191 the Mediterranean sea were also used  
192 ([http://www.upmc.fr/en/research/living\\_earth\\_and\\_environment\\_section/laboratories/villefr](http://www.upmc.fr/en/research/living_earth_and_environment_section/laboratories/villefranche_sur_mer_oceanography_laboratory_umr_7093.html)  
193 [anche\\_sur\\_mer\\_oceanography\\_laboratory\\_umr\\_7093.html](http://www.upmc.fr/en/research/living_earth_and_environment_section/laboratories/villefranche_sur_mer_oceanography_laboratory_umr_7093.html)). Additional data in the  
194 Chesapeake Bay, which is traditionally a turbid area (Wang *et al*, 2005), and data  
195 obtained from Ifremer and OPTIC-MED (2008) and OPTIC-PCAF (2004) cruises were also  
196 added as they provide some *in-situ* measurements on shores where SPM backscattering  
197 and CDOM absorption may be important.

198  
199 In-situ  $K_{d490}$  and  $K_{dPAR}$  values reported in public databases are calculated using Eq. 4  
200 and integrated over the first optical depth of  $E_{d490}$  ( $Z_{90} \sim 1/K_{d490}$ ) (Morel *et al.*, 2007). To  
201 validate either satellite-derived  $K_{d490}$  or  $K_{dPAR}$ , we produced “matchups”, i.e., data pairs of  
202 satellite-derived  $K_d$  and *in-situ* collocated in space (same pixel) and obtained during the  
203 same day. The satellite  $K_{d490}$  (Figures 2 to 6) is directly comparable to the *in-situ*  $K_{d490}$ .  
204 We estimated, using Ecolight and the IOP available for the matchups from NOMAD and  
205 Seabass dataset, a correction for  $K_{dPAR}(Z_{eu}) = 0.94 \cdot K_{dPAR}(Z_{90})$  as we do not have the  
206 irradiance profiles to re-estimate  $K_{dPAR}(Z_{eu})$ . This correction is applied to figures 7a and 9.  
207 For OPTICs (12 matchups of Figure 7) and Ifremer dataset (18 matchups of Figure 7), the  
208 higher values of Figure 7, we calculated  $K_{dPAR}(Z_{eu})$  from the irradiance profiles and Eq. 4.

209

210 Matchups are used to produce statistical comparisons for the two fields. Bias and  
211 Pearson correlation coefficient (R) for figures 2 to 7 are calculated on log-transformed  
212 data.

213

214

## 215 **B. Seagrass and Kelp data**

216

217 In-situ coverage of *P. oceanica* in Corsica and single beam sonar survey data  
218 acquired on rocky seabed covered by kelp (*L. hyperborea*) in Brittany (Meleder, 2010), are  
219 used to compare satellite-derived residual energy observed at the macrophytes lower  
220 limits to the known minimum thresholds reported in the literature. Six sites were selected  
221 by Ifremer according to accurate knowledge of species distribution and state of  
222 conservation, and the availability of an accurate bathymetry (resolution of 100m  
223 horizontally and 1 to 5 meters vertically).

224

## 225 **IV. Satellite data**

226

227 MERIS Level 2 Reduced Resolution (RR, 1km resolution) data were used to match up  
228 with *in-situ* for the validation exercise. MERIS Full Resolution (FR) data were used to  
229 provide temporal means of Zeu and  $K_{dPAR}$  over Europe. Coastal areas are characterised  
230 by strong gradients of Chl-a and SPM which strongly affect the absorption and scattering  
231 of light. Therefore, the use of FR data when available is clearly relevant. The level 2

232 MERIS RR archive is available at ACRI-ST and MERIS FR data for Europe were  
233 downloaded from ESA facilities. Pixels flagged (MERIS Level 2 Detailed Processing  
234 Model) as CLOUD and HIGLINT were discarded. FR daily nLw were then projected on a  
235 regular grid of 250\*250m<sup>2</sup>. Daily fields of  $K_{d490}$  and  $K_{dPAR}$  were subsequently calculated  
236 from nLw and temporally averaged over the period 2005 to 2009 as required by the  
237 EuseaMap project. Daily mean PAR (in mol.photons.d<sup>-1</sup>.m<sup>-2</sup>) was evaluated using the  
238 algorithm developed by Frouin in 1989 and recently updated in 2011 for MERIS using  
239 Level 1 RR. The daily fields are averaged temporally over the period 2005 to 2009. Then  
240 the temporal averaged mean PAR is attenuated using the averaged  $K_{dPAR}$  at 250 m  
241 resolution and (Eq. 3) to provide an estimation of residual PAR in the water column in  
242 mol.photons.m<sup>-2</sup>.d<sup>-1</sup>.

243

## 244 **V. Results**

### 245 **A. Evaluation of existing $K_{d490}$ model compared to our in-situ dataset.**

#### 246 **Mueller's algorithm**

247

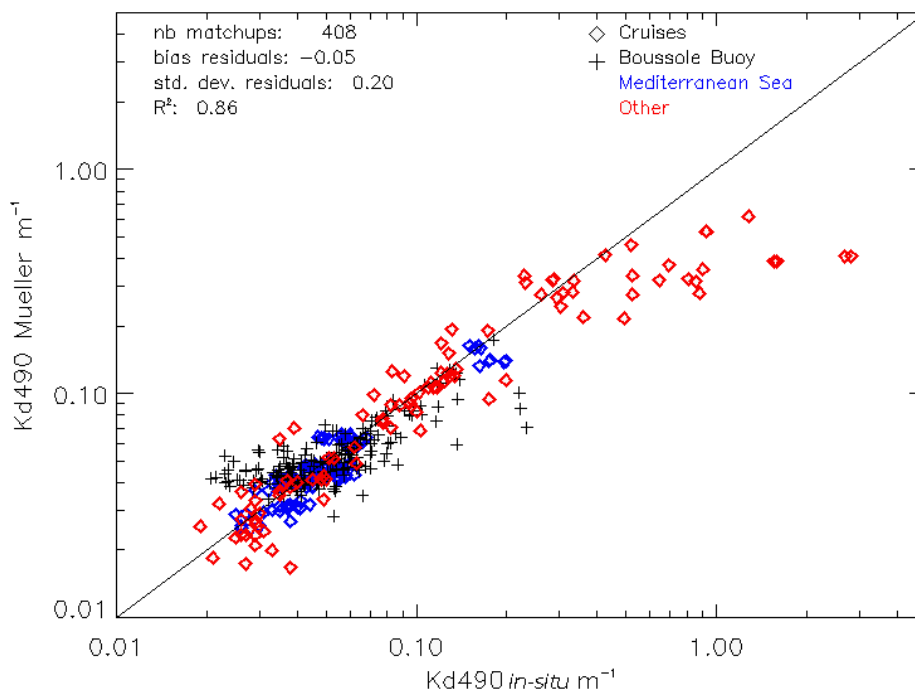
248 Mueller (2000) proposed an empirical model for non-turbid waters based on the ratio  
249 of the nLw at wavelengths 490 and 555 nm, i.e:

$$250 \quad K_{d490} = K_{w490} + A(nL_{w490} / nL_{w555})^B \quad (5)$$

251

252  $K_{w490} = 0.016 \text{ m}^{-1}$  is the diffuse attenuation coefficient for pure water. A was set initially  
253 to 0.15645 and B to -1.5401. Werdell (2005) updated (Eq. 5) to improve the algorithm

254 performance for the clearest ocean waters.  $K_{w490}$  was suppressed and A and B values  
255 were set respectively to 0.1853 and -1.349.



256

257

Figure 2: Mueller's  $K_{d490}$  vs *in-situ* .

258

259 Figure 2 shows that Mueller's  $K_{d490}$  estimation is accurate for clear water ( $K_{d490} < 0.2$   
260  $m^{-1}$ ). Above  $0.2 m^{-1}$  the algorithm saturates and the  $K_{d490}$  is clearly under-estimated  
261 compared to the dataset used. 'Other' in Figure 2 represents matchups not collected in the  
262 Mediterranean Sea. From this same dataset, the number of matchups may vary as we  
263 progress from Figure 2 to 7 as the spectral bands used and the algorithms may be  
264 different.

265

266

267 **Morel's approach**

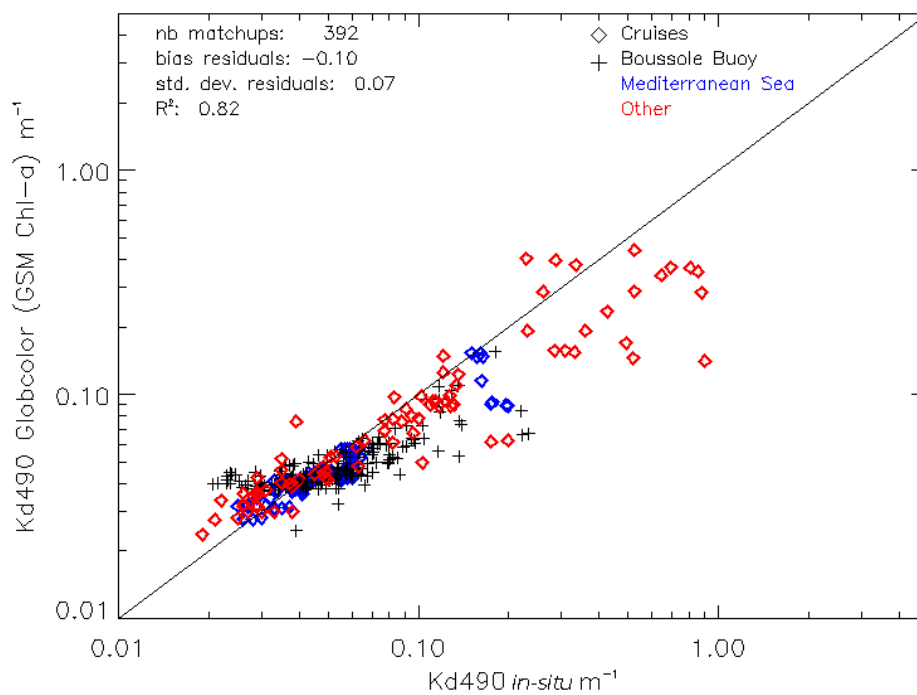
268

269 An empirical  $K_{d490}$  model based on chlorophyll-a concentration has been proposed by  
270 Morel in 2004. This model has been recently revised (Morel *et al.*, 2007) using *in-situ*  
271 measurements from the NASA Bio-Optical Marine Algorithm Dataset (NOMAD) (Werdell *et*  
272 *al.*, 2005). The revised formula is given as:

273

274 
$$K_{d490} = 0.0166 + 0.0773[Chl]^{0.6715} \quad (6)$$

275



276

277 **Figure 3: Morel's  $K_{d490}$  vs *in-situ***

278

279 Figure 3 shows that for  $K_{d490} < 0.2 m^{-1}$ , the estimated  $K_{d490}$  fits the *in-situ* retrievals.

280 For turbid  $K_{d490} > 0.3 m^{-1}$  the model underestimates the attenuation. We recall that the

281 Mueller and Morel's algorithms have been calibrated and dedicated for open sea clear  
282 waters.

283

284

### 285 **Lee's semi-analytical algorithm**

286

287 Lee *et al.* (2005) proposed a semi-analytical approach to derive the mean  $K_d(\lambda)$   
288 based on a radiative transfer model. The model has been revised recently (Lee *et al.*,  
289 2007), and  $K_d(\lambda, 10\%)$  i.e. integrated from the surface to the depth where  $(E(z, \lambda) = 10\%$   
290  $E_0(\lambda))$  can be written as (Lee *et al.*, 2005a):

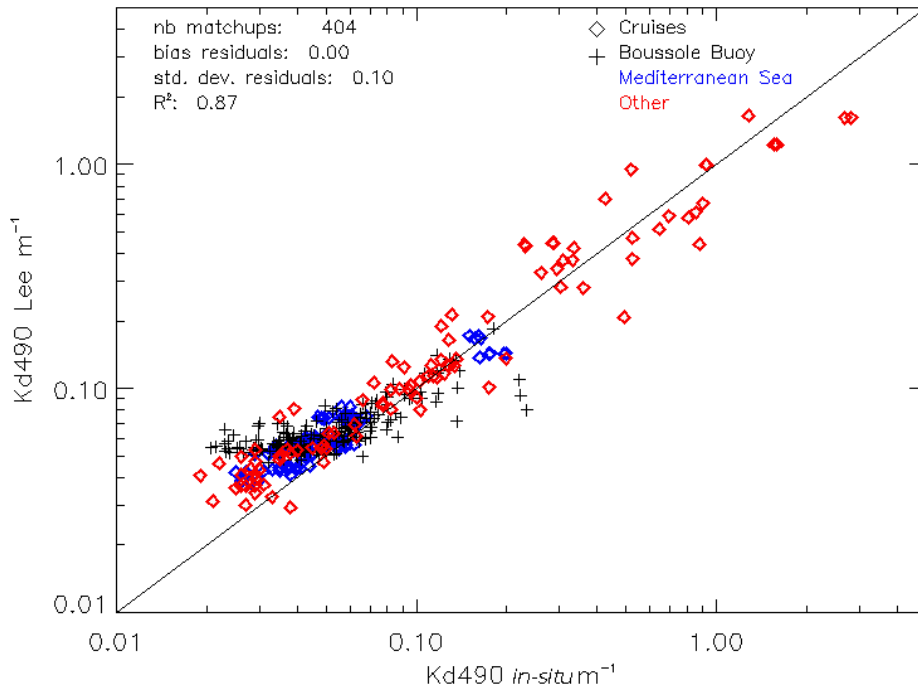
291

$$292 \quad K_d(\lambda, E10\%) = (1 + 0.005 \cdot \theta_s) \cdot a(\lambda) + 4.18 \cdot (1 - 0.52 \cdot e^{-1.8 a}) \cdot b_b(\lambda) \quad (7)$$

293

294 Where  $\theta_s$  is the solar-zenith angle in the air,  $a(\lambda)$  the total absorption at  $\lambda$  and  $b_b(\lambda)$  the  
295 total backscattering at  $\lambda$ . It is interesting to note that the semi-analytical approach  
296 developed by Lee allows the derivation of  $K_d$  at any wavelength. In our case, at  $\lambda = 490$   
297 nm,  $K_{d490}$  is derived from Eq. (7) and the absorption and backscattering coefficients at 490  
298 nm,  $a(490)$  and  $b_b(490)$  are themselves calculated using Lee's QAA v5 algorithm applied to  
299 the MERIS Rrs at wavelengths 443, 490, 555, and 670 nm.

300



301

302

Figure 4: Lee's  $K_{d490}$  vs *in-situ*

303

304

We observe in Figure 4 a good agreement between the satellite-derived  $K_{d490}$  and *in-*

305

*situ* measurements between 0.06 and 1  $m^{-1}$ . For very clear waters,  $K_{d490}$  tends to be

306

overestimated when compared to our *in-situ* dataset. For *in-situ*  $K_{d490}$  greater than 0.08  $m^{-1}$

307

<sup>1</sup> the estimated  $K_{d490}$  compares well with the *in-situ* data.

308

309

310

## **B. From $K_{d490}$ to $K_{dPAR}$**

311

312

To derive the relationships between  $K_{d490}$  and  $K_{dPAR}$ , we have calculated using (Eq. 2b)

313

the PAR values at the selected matchups at any depth, using a 0.1m step for  $z$ , until

314

$PAR(z) = 1\% PAR(0)$ .  $K_d(\lambda)$  at the wavelengths 412, 443, 489, 509, 559, 620, 664, 709

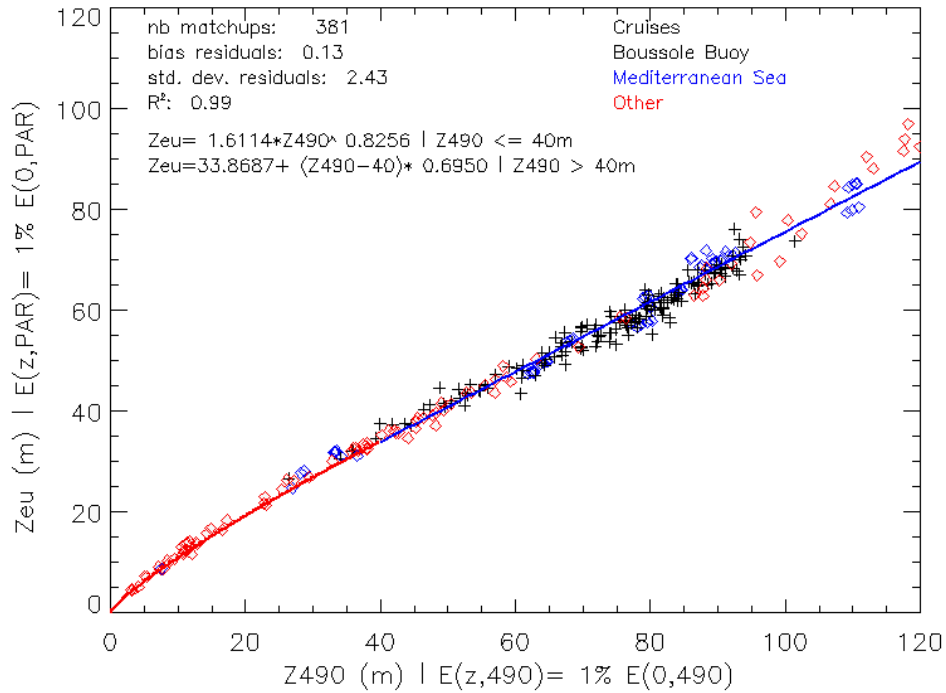
315 were derived from Eq. 7 and applied to MERIS Rrs.  $E_d(\lambda, z)$  were evaluated using equation  
316 (8) (Gordon and Wang 1983), the theoretical extra-terrestrial solar irradiances  $F_0(\lambda)$ , the  
317 Rayleigh optical thicknesses  $T(\lambda)$  and the theoretical values of the ozone transmittance  
318  $T_{O3}(\lambda)$ .

$$319 \quad E_0(z, \lambda) = F_0(\lambda) \cdot \exp^{-T(\lambda)/2} \cdot T_{O3}(\lambda) \quad (8)$$

320

321 Two relationships were derived between  $Z_{eu}$  and the depth at which  
322  $E(Z, 490) = 1\% E(0, 490)$ ,  $Z_{490}$ , using the  $L_w$  observed at the in-situ matchups (Figure 5). The  
323 two relationships between  $K_{dPAR}$  and  $K_{d490}$  are directly derived from the two relationships  
324 between  $Z_{eu}$  and  $Z_{490}$ . Relating  $K_{dPAR}$  to  $K_{d490}$  was not absolutely necessary as we could  
325 have integrated the spectral  $K_d$  provided by Lee using Eq. 2b. Nevertheless, we decided  
326 to propose a relationship between  $K_{dPAR}$  and  $K_{d490}$  as this link is meaningful and useful to  
327 derive  $K_{dPAR}$  from several  $K_{d490}$  *in-situ* datasets that are available. The threshold of 40 m for  
328  $Z_{490}$  ( $K_{d490} = 0.115 \text{ m}^{-1}$ ) was set arbitrary to separate clear from turbid waters.

329



330

331 Figure 5: Euphotic depth (Zeu) related to Z<sub>490</sub> (depth Z at which E(Z,490)=1%E(0,490))

332 for the selected matchups.

333

334 An exponential model is fitted for turbid waters (Z<sub>490</sub> < 40m) and a linear model for

335 clear water (Z<sub>490</sub> >= 40m). The proposed equations between K<sub>dPAR</sub> and K<sub>d490</sub> are shown in

336 Figure 6 (Eq. 9a in blue and 9b in red).

337

338  $K_{dPAR} = 4.6051 \cdot K_{d490} / (6.0700 \cdot K_{d490} + 3.200)$ , for  $K_{d490} \leq 0.115 \text{ m}^{-1}$  (9a)

339  $K_{dPAR} = 0.8100 \cdot K_{d490}^{0.8256}$ , for  $K_{d490} > 0.115 \text{ m}^{-1}$  (9b)

340

341 Morel (2007) expressed K<sub>dPAR</sub> as a function of K<sub>d490</sub> for clear waters :

342  $K_{dPAR} = 0.0665 + 0.874 \cdot K_{d490} - 0.00121 / K_{d490}$  (10)

343

344

345 Similar approaches to Eq. 9b have been recently developed by Wang & Son (Eq. 11,  
346 2009) and Pierson & Kratzer (Eq 12, 2008) for respectively the Cheasapeake Bay turbid  
347 waters and Baltic Sea, where CDOM absorption is important.

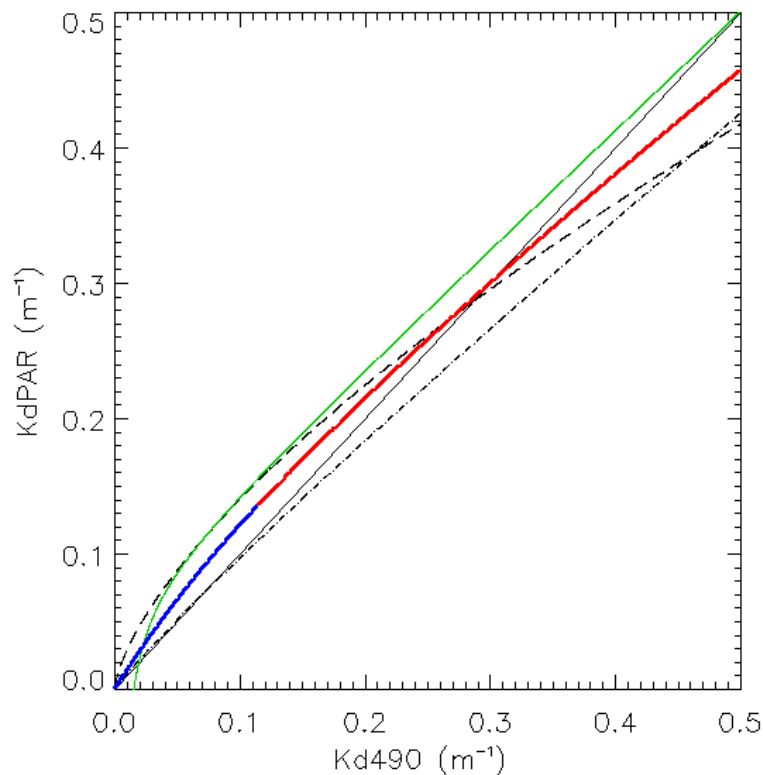
348 
$$K_{dPAR} = 0.8045.K_{d490}^{0.9170} \quad (11)$$

349 
$$K_{dPAR} = 0.6677.K_{d490}^{0.6763} \quad (12)$$

350

351 Relationships between  $K_{dPAR}$  and  $K_{d490}$  directly depend of [Chl-a],  $a_{cdom}$  and [SPM]. In  
352 clear waters  $K_{d490}$  values are less than  $K_{dPAR}$  values as the attenuation is greatest in the  
353 red with a resulting stronger PAR attenuation (which includes the red). In coastal areas,  
354 Kratzer (2007) suggests that increasing  $a_{cdom}$  has the result of increasing more rapidly  
355  $K_{d490}$  than  $K_{dPAR}$ .

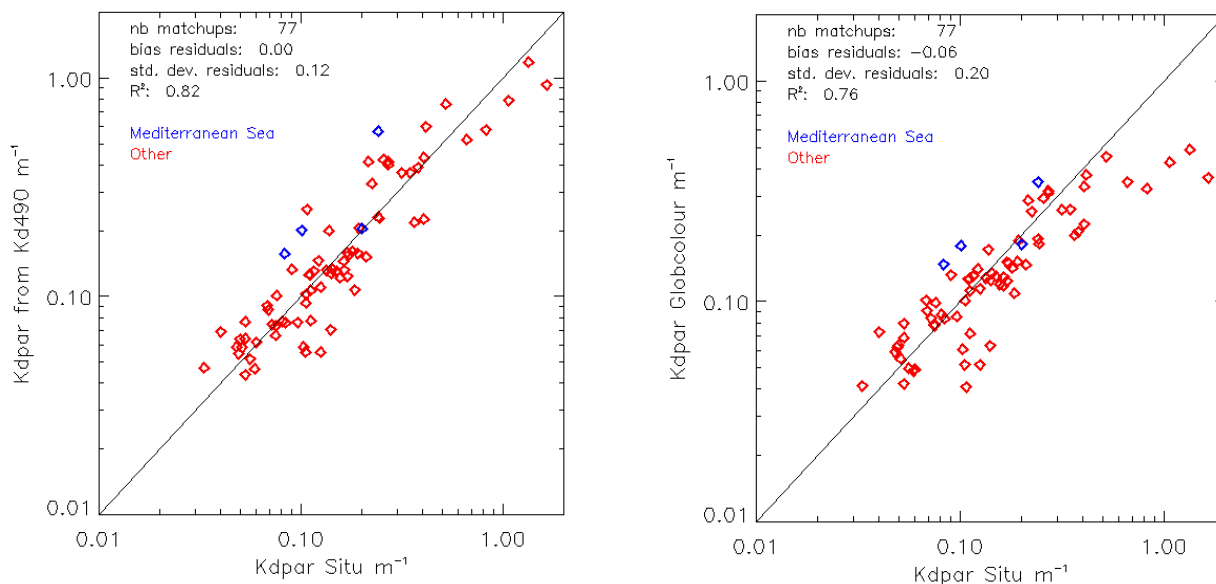
356



357

358 Figure 6: Relationships between  $K_{dPAR}$  and  $K_{d490}$ . Blue curve for clear waters (Eq. 9b),

359 red for coastal waters (Eq. 9a). The green curve shows the Morel (Eq. 10) for clear waters.  
 360 The short black dotted the Wang & Son's relationship for the Chesapeake bay (Eq. 11) and  
 361 long black dashed line the relationship derived by Pierson & Kratzer for the Baltic Sea (Eq.  
 362 12).



364 Figure 7: a) satellite-derived  $K_{dPAR}$  from equations (Eq. 9a and b) vs *in-situ*  $K_{dPAR}$ . b)  
 365 Globcolour standard  $K_{dPAR}$  (Eq 10).

366  
 367 Figure 7 shows the scatterplot of the estimated  $K_{dPAR}$  (Fig 7a) and the Globcolour (Fig.  
 368 7b) vs *in-situ* data. The estimated  $K_{dPAR}$  is higher than the case 1 Globcolour standard  
 369 algorithm for values greater than 0.3 (Figure 6). Although the number of matchups  
 370 available is small for  $K_{dPAR} > 0.3 \text{ m}^{-1}$  we can observe the saturation effect on the standard  
 371  $K_{dPAR}$ . The number of available  $K_{dPAR}$  matchups is too small (Figure 7, 77 matchups) and  
 372 we propose therefore an alternative validation using Ecolight simulations. The Ecolight  
 373 configuration is provided in annex A. To obtain a realistic distribution of the IOPs we start  
 374 from those gathered in the NOMAD dataset. The NOMAD dataset does not provide [SPM]

375 and an estimation of this concentration was done using Babin (2003):

376

$$377 \quad [\text{SPM}] = 1.73 / 0.015 \cdot b_{\text{bp}443} \quad (14)$$

378

379  $B_{\text{bp}443}$  is the particular backscattering measured at 443 nm. The sun zenith angle,  $\Theta_s$ ,

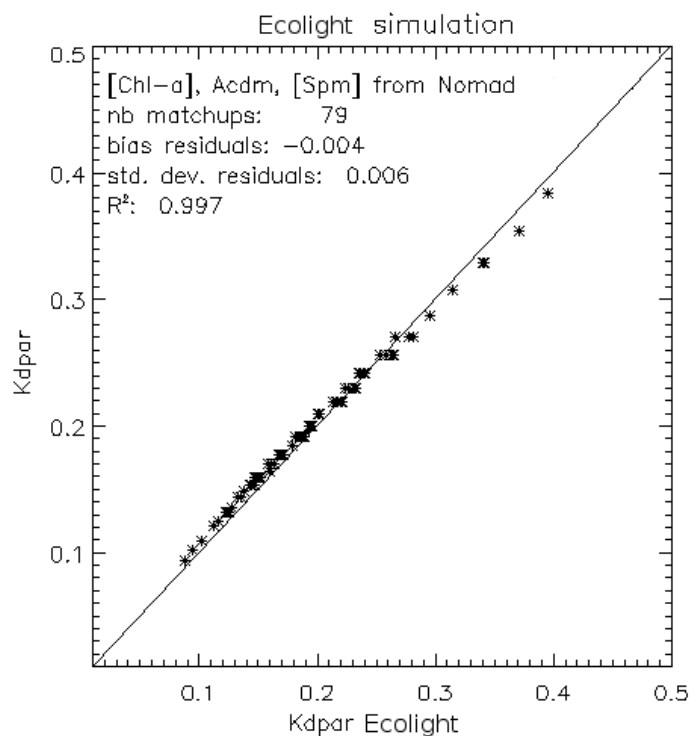
380 a required input parameter for Ecolight, was estimated for each *in-situ* data using the date,

381 time, longitude and latitude. Finally the satellite-derived  $K_{\text{dPAR}}$  is compared to the  $K_{\text{dPAR}}$

382 estimated using Ecolight ( $K_{\text{dPAR}}$  is calculated from the PAR provided in the Ecolight output

383 files and averaged using Eq. 4 and the depth at which  $E(z) = 1\% E_0$ ).

384



385

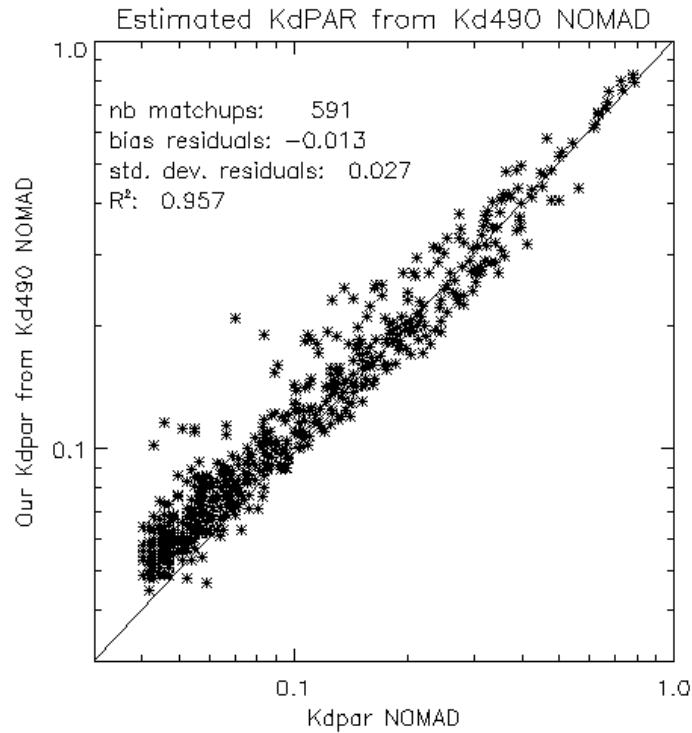
386 Figure 8: Scatterplot between the Ecolight simulations and estimated  $K_{\text{dPAR}}$  based on

387  $K_{\text{d}490}$  by Lee *et al.* (2005).

388

389 Eq. 9 can also be used to derive an estimate of  $K_{\text{dPAR}}$  from  $K_{\text{d}490}$ . Figure 9 shows a

390 comparison for the NOMAD dataset between the  $K_{dPAR}$  estimated from the *in-situ*  $K_{d490}$  and  
391 the corresponding *in-situ*  $K_{dPAR}$ , i.e. a validation of Eq. 9 and Figure 6.  
392



393

394 Figure 9: Estimated  $K_{dPAR}$  from *in-situ*  $K_{d490}$  measurements compared to *in-situ*  $K_{dPAR}$ .

395

396 Figure 9 shows an overestimation for the very clear waters. As Lee's algorithm slightly  
397 overestimated  $K_{d490}$  for clear waters (Figure 4) and  $K_{dPAR}$  is derived from satellite data and  
398 Lee's spectral  $K_d$ , this slight overestimation occurs for  $K_{dPAR} < 0.1 \text{ m}^{-1}$ , i.e.  $Z_{eu} > 46\text{m}$ . For  
399  $K_{dpar}$  greater than  $0.1 \text{ m}^{-1}$  the estimated value fits to the in-situ data.

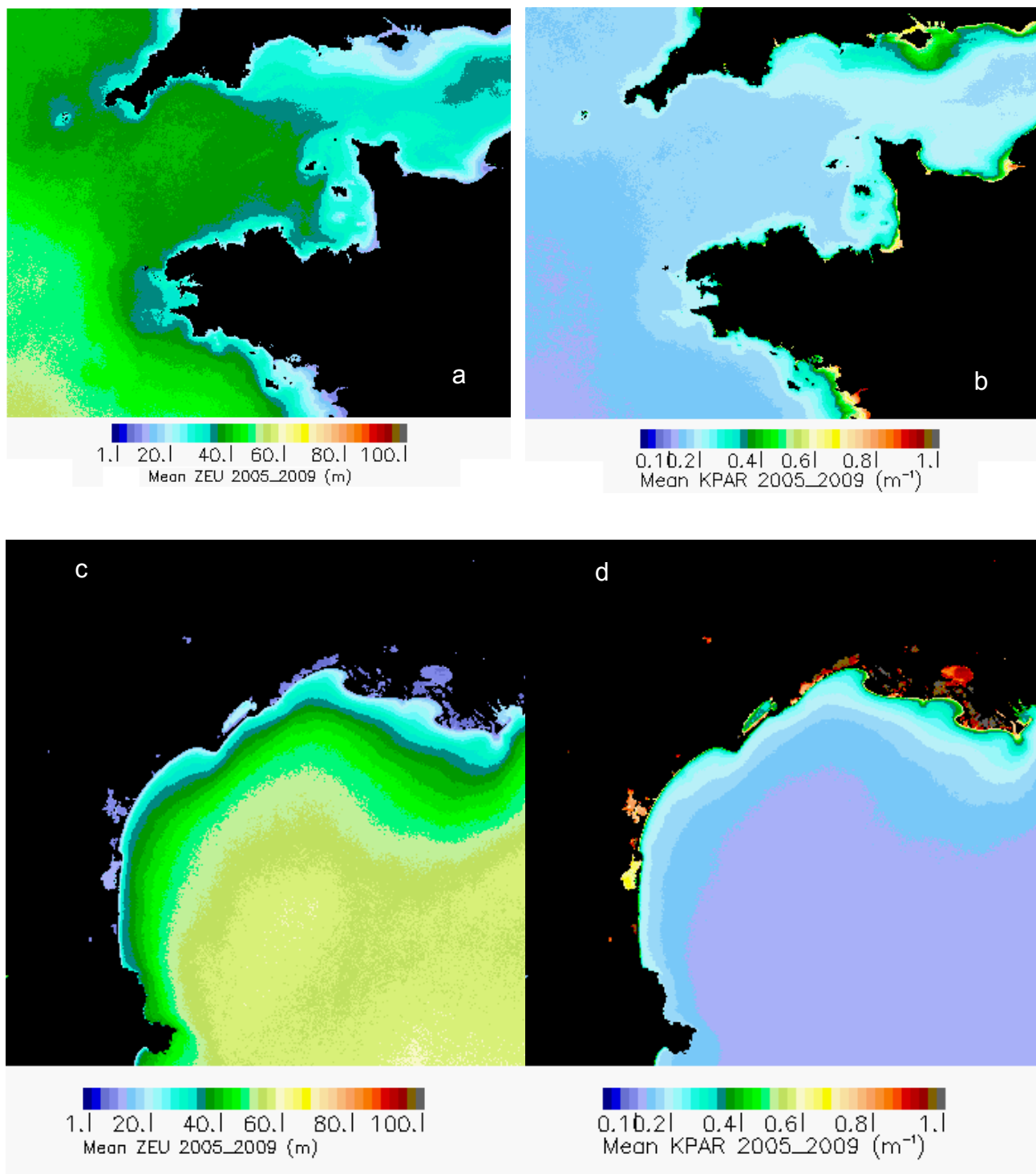
400

### 401 **C. High resolution maps of $Z_{eu}$ and $K_{dPAR}$ .**

402

403 Figure 10 shows the temporal mean of  $K_{dPAR}$  and  $Z_{eu}$  for Brittany and the Gulf of Lions

404 at 250m resolution. The covered area (Europe) by the EuSeaMap project was divided in  
405 25 zones (not shown).  
406



407 Figure 10: Mean of  $Z_{eu}$  and  $K_{dPAR}$  at 250 m resolution over the period 2005-2009 for

408 the Brittany (a and b) and the Gulf of Lions (c and d).

409

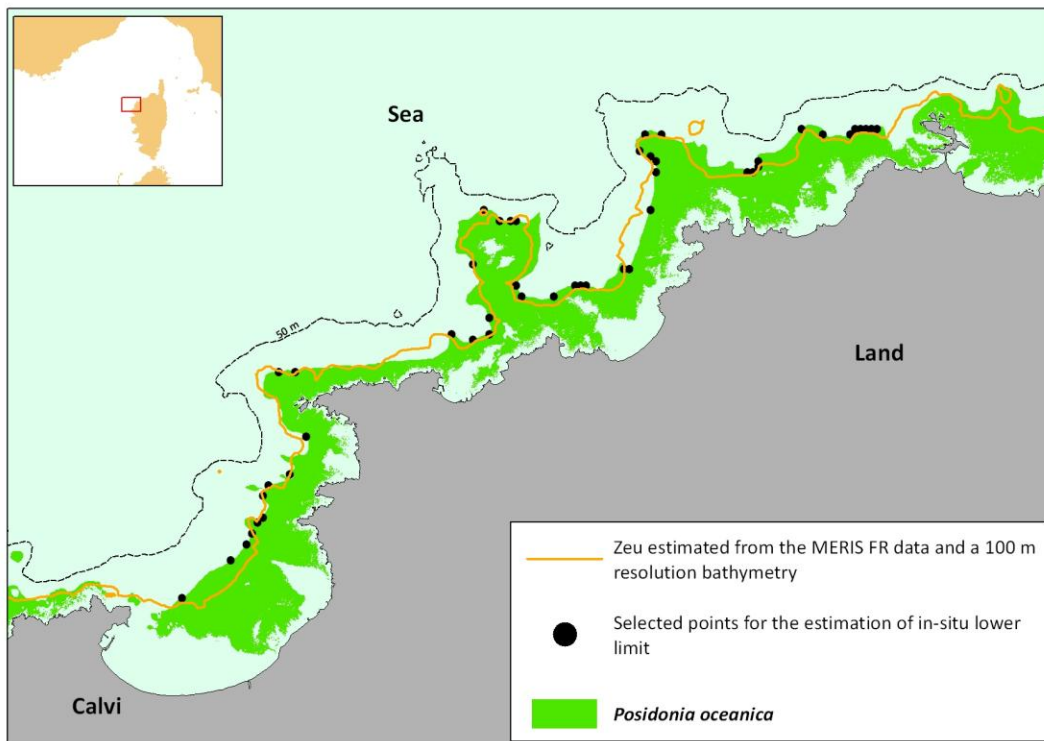
#### 410 **D. Application to seabed habitat mapping**

##### 411 ***P. oceanica* in Corsica**

412

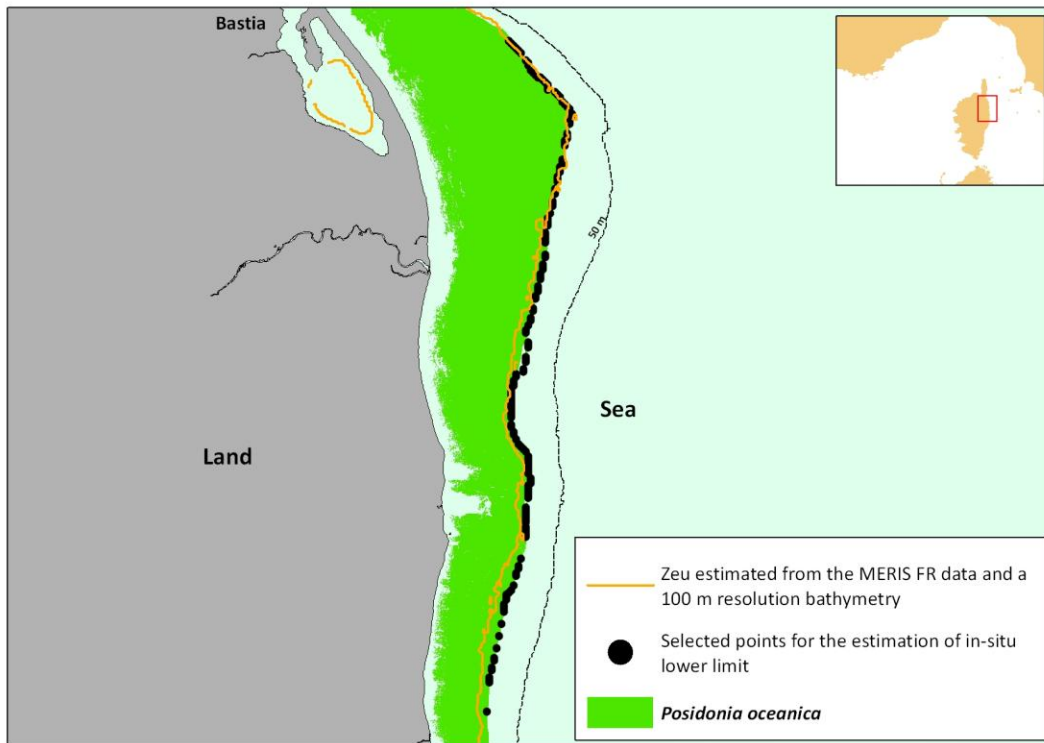
413 In Corsica three sites where *P. oceanica* meadows are known to be in a natural state  
414 were selected for comparison. Figure 11 shows the distribution of *P. oceanica* at two sites  
415 in north-west (Calvi) and north-east (south Bastia) Corsica. The orange line shows Zeu  
416 (1%  $E_0$ ) estimated from MERIS 250 m over the period 2005-2009. It is interesting to note  
417 that the lower extension for *P. oceanica* follows the satellite-derived Zeu.

418



419

420



421

422 Figure 11: Distribution of *P. oceanica* compared to Zeu derived from MERIS RR and  
 423 FR daily data from 2005 to 2009 at Calvi a) and Bastia b).

424

425

426 Gattuso (2006) proposed a light range of  $0.1$  to  $2.8 \text{ mol.photons.m}^{-2}.\text{d}^{-1}$  for the  
 427 minimum requirements of *P. oceanica*. Table 2 shows for the 3 selected sites the observed  
 428 value in percentage of the surface irradiance and energy at the lower limit of the *Posidonia*  
 429 beds. Using a GIS software, in situ points (black dots, Figure 11) were selected manually  
 430 on fine scale *Posidonia* maps at locations representing the deep boundary of the  
 431 meadows. Statistics (Table 2) were computed for depth, percentage of the surface  
 432 irradiance and energy by retrieving at these locations the values of pixels from respectively  
 433 a 100m resolution depth DTM, the temporal mean at 250 m resolution of  $K_{d\text{PAR}}$  and the  
 434 temporal mean at 1km resolution of PAR. The observed mean values, weighted means for  
 435 the 3 sites by the number of observations, are  $0.94\%$  and  $0.26 \text{ mol.photons.m}^{-2}.\text{day}^{-1}$  for *P.*

436 *oceanica*. These values are very close to the 1 % threshold and in the lower part of the  
437 energy range proposed by Gattuso (2006).

438

439 Table 2: Statistics of fraction of the surface light and corresponding energy in  
440 mol.photons.m<sup>-2</sup>.d<sup>-1</sup> observed at the lower limit of *P. oceanica* beds.

441

442 **Aléria**, depth DTM accuracy: 1m

	Min	<b>Mean</b>	Max	Stdev	Nb points
<b>% E<sub>0</sub></b>	0.46	<b>1.15</b>	1.92	0.20	165
<b>mol.photons.m<sup>-2</sup>.day<sup>-1</sup></b>	0.13	<b>0.33</b>	0.56	0.06	165
<b>Depth (m)</b>	26.0	<b>31.8</b>	37.0	2.68	165

443

444 **South Bastia**, depth DTM accuracy: 1m

	Min	<b>Mean</b>	Max	Stdev	Nb points
<b>% E<sub>0</sub></b>	0.4	<b>0.73</b>	1.24	0.24	171
<b>mol.photons.m<sup>-2</sup>.day<sup>-1</sup></b>	0.12	<b>0.22</b>	0.36	0.06	171
<b>Depth (m)</b>	33.0	<b>35.4</b>	38.0	1.1	171

445

446 **Calvi** depth DTM accuracy: 5m

	Min	<b>Mean</b>	Max	Stdev	Nb points
<b>% E<sub>0</sub></b>	0.44	<b>0.96</b>	2.04	0.12	48
<b>mol.photons.m<sup>-2</sup>.day<sup>-1</sup></b>	0.13	<b>0.28</b>	0.60	0.04	48
<b>Depth (m)</b>	28.0	<b>31.0</b>	33.0	1.6	48

447

448

449

## 450 **Kelp in Brittany**

451

452 In the same manner as the previous analysis, we have evaluated the minimum light  
453 requirements for kelp using single beam sonder acoustic data acquired in 2006 and 2007  
454 at three sites in Brittany (les Abers in north Brittany, îles de Glénan and île de Groix in  
455 south Brittany). The bathymetry used here is calculated from the hydrographic zero, which  
456 in France corresponds to the lowest observed sea level. While in the Mediterranean Sea  
457 the tide range is very low, it can reach several meters in Brittany. Therefore the half of the  
458 annual mean tide value at Brest (0.5\*6.1m, Service Hydrographique et Océanographique  
459 de la Marine, SHOM) was added.

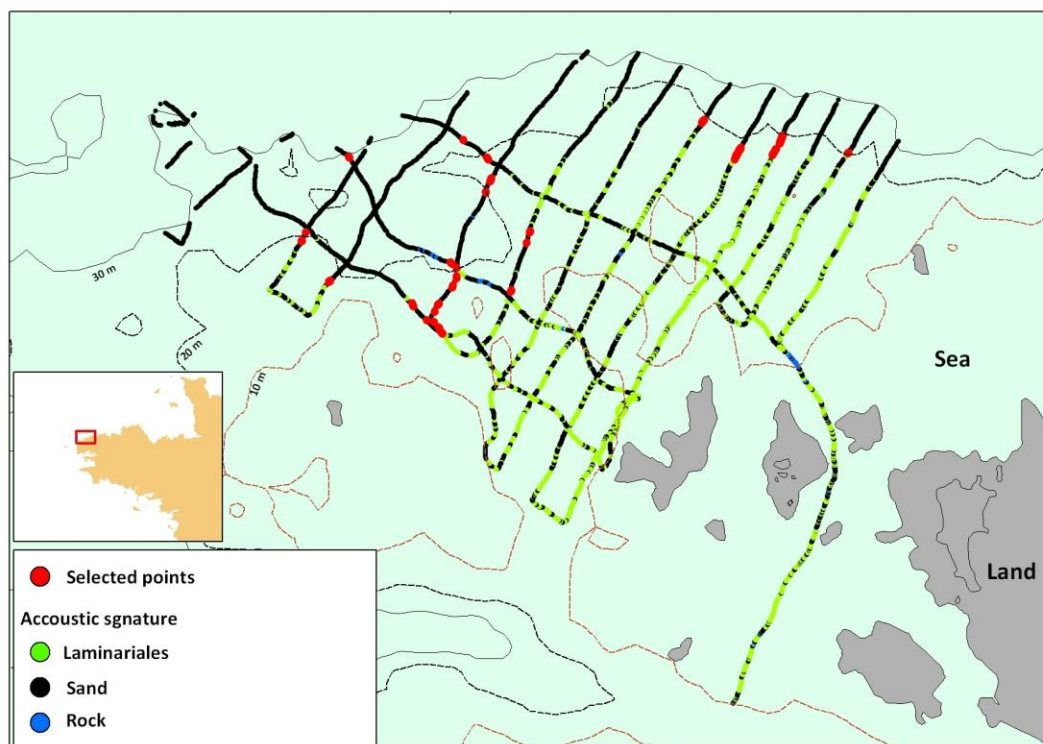
460

461 Figure 12 shows the distribution of *L. hyperborea* in the French Abers. Kelp forest  
462 presence was obtained by echo-integrating the acoustic signal (Meleder, 2010), which  
463 enables distinguishing dense kelp forest from sparse kelp or bare rock. The sonder also  
464 provided *in situ* depth measurements reduced for tide, resulting in an accurate estimate of  
465 the depth (with an uncertainty of 0.5m). The values observed for the minimum in les Abers  
466 (mean of 2.3%) is significantly higher for the two other sites. This can be explained by the  
467 hydrodynamic energy regime at the seabed which differs greatly between the Channel and  
468 south Brittany. Kain (1971, 1976) proposed a minimum percentage of incidental light  
469 ranges from 1% to 1.9 % for *L. hyperborean* and Lüning (1979, 1990), 0.7% and 70 mol.m<sup>-2</sup>.year<sup>-1</sup>  
470 for this specie, i.e. 0.19 mol.photons.m<sup>-2</sup>.d<sup>-1</sup>.

471

472 The calculated mean weighted values are 1.73% and 0.42 mol.photons.m<sup>-2</sup>.d<sup>-1</sup>, in the

473 range expressed in percent proposed by Kain and slightly higher than the threshold  
 474 proposed by Lüning.



475  
 476 Figure 12: Single-beam survey lines (thick lines) for the site Abers. Green dots denote  
 477 the presence of kelp forest. Red dots are deepest occurrences of kelp forest.

478  
 479 Table 3: Statistics of the fraction of surface light and the corresponding energy in  
 480 mol.photons.m<sup>-2</sup>.d<sup>-1</sup> observed at the lower limit of *L. hyperborea* in Brittany.

481  
 482 **Abers**

	Min	<b>Mean</b>	Max	Stdev	Nb points
<b>% E<sub>0</sub></b>	1.72	<b>2.3</b>	2.74	0.43	74
<b>mol.photons.m<sup>-2</sup>.day<sup>-1</sup></b>	0.42	<b>0.57</b>	0.68	0.11	74
<b>Depth (m)</b>	21.1	<b>22 .0</b>	24.7	0.65	74

484

485 **Glénan**

	Min	<b>Mean</b>	Max	Stdev	Nb points
<b>% E<sub>0</sub></b>	0.39	<b>0.85</b>	1.24	0.41	32
<b>mol.photons.m<sup>-2</sup>.day<sup>-1</sup></b>	0.12	<b>0.20</b>	0.39	0.10	32
<b>Depth (m)</b>	26.0	<b>28.2</b>	32.1	1.96	32

486

487

488 **Groix Sud**

	Min	<b>Mean</b>	Max	Stdev	Nb points
<b>% E<sub>0</sub></b>	1.00	<b>1.25</b>	1.54	0.29	28
<b>mol.photons.m<sup>-2</sup>.day<sup>-1</sup></b>	0.24	<b>0.31</b>	0.38	0.08	28
<b>Depth (m)</b>	19.1	<b>19.9</b>	21.0	0.60	28

489

490

491 **VI. Conclusions:**

492

493 We propose two relationships between the mean  $K_{dPAR}$ , integrated over the euphotic  
 494 layer, and the  $K_{d490}$  estimated according to Lee *et al.* (2005), for very clear waters ( $K_{dPAR} <$   
 495  $0.115 \text{ m}^{-1}$ ) and turbid waters ( $K_{dPAR} \geq 0.115 \text{ m}^{-1}$ ). The empirical relationship for coastal  
 496 areas suggests a correction to the underestimation of  $K_{dPAR}$  by the standard Globcolour  
 497 case 1 algorithm, and also provides an estimation of the  $K_{dPAR}(Z_{eu})$  from the *in-situ*  $K_{d490}$ .  
 498 Satellite derived  $K_{d490}$  and  $K_{dPAR}$  have been validated using available matchups between  
 499 the MERIS data and *in-situ* measurements and Ecolight simulations. Results of validation

500 suggest that the Lee *et al.* (2005) algorithm derived for MERIS is valid for estimation of  
501  $K_{d490}$  and the subsequent  $K_{dPAR}$  in coastal areas.

502

503 The mean values of the observed threshold for the three selected sites in Corsica and  
504 *P. oceanica* were 0.94% and 0.13 mol.photons.m<sup>-2</sup>.d<sup>-1</sup> for *P. oceanica*. These estimates are  
505 very close to the 1% definition of Zeu and in the lower limit of the energy range proposed  
506 by Gattuso (2006). For *L. hyperborea* surveys in Brittany, our estimated values from the  
507 satellite data were 1.73% and 0.42 mol.photons.m<sup>-2</sup>.d<sup>-1</sup>, in the range (1-1.9%) proposed by  
508 Kain (1971, 1976) and slightly higher than the energy threshold proposed by Lüning (0.7  
509 %, 0.19 mol.photons.m<sup>-2</sup>.d<sup>-1</sup> 1979, 1990). The bathymetry used in this work is calculated  
510 from the hydrographic zero, which in France corresponds to the lowest observed level of  
511 the sea. The influence of the tide has been considered in Brittany by adding a half mean  
512 tide level. Bowers (2009) showed also that because of tide and non-linearity of the light  
513 attenuation, the light gained at low tide exceeds the loss at high tide leading to a deeper  
514 colonisation of the specie in such areas. Therefore, future works will integrate accurate  
515 local estimations of annual mean tide values.

516

517 The estimation of minimum light requirements in mol.photons.m<sup>-2</sup>.d<sup>-1</sup>, a true physical  
518 quantity, is meaningful compared to an estimation expressed in fraction of surface energy.  
519 This residual energy reaching the bottom at high resolution is also good candidate as input  
520 parameter in the predictive modelling of seabed habitats such as proposed by Meleder  
521 (2010).

522

523

524 **Acknowledgements:** This work was funded by the EuseaMAP project

525 <http://www.jncc.gov.uk/page-5027> of the European Commission's Directorate-General for  
526 Maritime Affairs and Fisheries. The authors thank the SHOM and Frédéric Jourdin for  
527 providing OpticMed data and high resolution DTMs Michel Lunven from Ifremer for the  
528 provision of PAR profiles on the French shores, Robert Frouin for the provision of a revised  
529 version of the PAR estimation using MERIS data, Zhong-Ping Lee for useful advice and  
530 the Medbenth project for access to Mediterranean seagrass maps and Nick Stephens,  
531 from the Plymouth Marine Laboratory, for additional comments.

532

533

## 534 **VII. References**

535

536 Baker, K. S., and Frouin R. (1987). Relation between photosynthetically available  
537 radiation and total insolation at the ocean surface under clear skies. *Limnology and*  
538 *Oceanography*, 32:1370-1377.

539

540 Babin, M., Stramski, D., Ferrari, G.M., Claustre, H., Bricaud, A., Obolensky, G., and N.  
541 Hoepffner (2003). Variations in the light absorption coefficients of phytoplankton, non-algal  
542 particles, and dissolved organic matter in coastal waters around Europe, *Journal of*  
543 *Geophysical Research*, 10.1029

544

545 Bowers, D.G and Brubaker, J.M (2010), Tidal amplification of seabed light, *Journal of*  
546 *Geophysical Research*, 115, C09008.

547

548 Cahoon, L. B., Beretich, G. R., Thomas, C. J., and McDonald, A. M. (1993). Benthic

549 microalgal production at Stellwagen Bank, Massachusetts Bay, USA. *Marine Ecology*  
550 *Progress Series*, 102(1–2):179-185.

551

552 Carter, C.M., Ross, A.H., Schiel, D.R., Howard-Williams, C. and Hayden, B., (2005).  
553 In situ microcosm experiments on the influence of nitrate and light on phytoplankton  
554 community composition. *Journal of Experimental Marine Biology and Ecology*, 326:1-13.

555

556 Claustre, H. and Maritorena, S. (2003). The many shades of ocean blue. *Science*, 302:  
557 1514-1515.

558

559 Devlin, M.J., Barry, J., Mills, D.K., Gowen, R.J., Foden, J., Sivyer, D., Greenwood, N.,  
560 Pearce, D., and Tett, P. (2009). Estimating the diffuse attenuation coefficient from optically  
561 active constituents in UK marine waters. *Estuarine, Coastal and Shelf Science*, 82(1) :73-  
562 83.

563

564 Esaias, W.E., Abbott, M.R., Barton, I., Brown, O.B., Campbell, J.W., Carder, K.L.,  
565 Clark, D.K., Evans, R.H., Hoge, F.E., Gordon, H.R., Balch, W.M., Letelier, R., Minnett, P.J.  
566 (1998). An overview of MODIS capabilities for ocean science observations. *IEEE*  
567 *TRANSACTIONS ON GEOSCIENCE AND REMOTE SENSING*, 36(4):1250-1265.

568

569 Falkowski, P.G., Raven, J.A. (1997). Aquatic Photosynthesis. *Blackwell Science*, 349  
570 pp.

571

572 Frouin, R., Lingner, D. W., and Gautier C. (1989). A Simple Analytical Formula to  
573 Compute Clear Sky Total and Photosynthetically Available Solar Irradiance at the Ocean

574 Surface. *Journal of Geophysical Research*, 94(7): 9731-9742

575

576 Gattuso J.-P., Gentili B., Duarte C. M., Kleypas J. A., Middelburg J. J. & Antoine D.,  
577 2006. Light availability in the coastal ocean: impact on the distribution of benthic  
578 photosynthetic organisms and their contribution to primary production. *Biogeosciences*, 3:  
579 489-513.

580

581 Gohin Francis, Loyer S, Lunven Michel, Labry Claire, Froidefond J, Delmas Daniel,  
582 Huret Martin, Herbland Alain. (2005). Satellite-derived parameters for biological modelling  
583 in coastal waters: Illustration over the eastern continental shelf of the Bay of Biscay.  
584 *Remote Sensing of Environment*, 95(1): 29-46.

585

586 Gordon, H. R., & Morel, A. (1983). Remote assessment of ocean color for  
587 interpretation of satellite visible imagery: A review. *Springer-Verlag New York*, Vol. 114.

588

589 Gordon, H. R. and Wang M. (1994). Retrieval of water-leaving radiance and aerosol  
590 optical thickness over the oceans with SeaWiFS: a preliminary algorithm, *Applied Optic*,  
591 33(3): 443–452.

592

593 IOCCG Report 3. (2000). Remote sensing in Coastal and Other Optically-Complex  
594 Waters.

595

596 Jerlov, N. G. (1976). *Optical Oceanography*. New York: Elsevier, 118-122

597

598 Kirk, J.T.O. (1994). *Light and Photosynthesis in Aquatic Ecosystems*. Cambridge

599 *University Press.*

600

601 Kain, J. M. (1971). Continuous recording of underwater light in relation to Laminaria  
602 distribution. *Marine Biology Symposium*. Cambridge Univ. Press, London, p. 335-346

603

604 Kain, J. M. (1976). The biology of Laminaria hyperborea. *Oceanography and Marine  
605 Biology Annual Review*, 17: 101-161

606

607 Lee, Z. P. (2009). KPAR: An ambiguous optical property. *Journal of Lake Sciences*,  
608 21:159-164.

609

610 Lee, Z.P., Lubac, B., Werdell, J., & Arnone, R. (2009). An update of the quasi-  
611 analytical algorithm (v5). IOCCG software report. [www.ioccg.org/groups/Software\\_OCA](http://www.ioccg.org/groups/Software_OCA).

612

613 Lee, Z. P., Carder, K. L., and Arnone, R. A. (2002), Deriving inherent optical properties  
614 from water color: a multiple quasi-analytical algorithm for optically deep waters. *Applied  
615 Optic*, 41: 5755-5772.

616

617 Lee, Z. P., Darecki, M., Carder, K., Davis, C., Stramski, D., and Rhea W. (2005).  
618 Diffuse attenuation coefficient of downwelling irradiance: An evaluation of remote sensing  
619 methods. *Journal of Geophysical Research*, 110, C02017.

620

621 Lee, Z. P., DU, K.P. and Arnone R. (2005). A model for the diffuse attenuation  
622 coefficient of downwelling irradiance. *Journal of Geophysical Research*, 110, C02016.

623

624 Lee, Z. P., Weideman, A., Kindle, J., Arnone, R., Carder, K., and Davis, C. (2007).  
625 Euphotic zone depth: Its derivation and implication to ocean-color remote sensing. *Journal*  
626 *of Geophysical Research*, 112, C03009.

627

628 Lewis, M., Carr, M., Feldman, G., Esaias, W. E. , and McClain, C. R. (1990). Influence  
629 of penetrating solar radiation on the heat budget of the equatorial Pacific ocean. *Nature*,  
630 347: 543-545.

631

632 Lüning, K. (1979). Growth strategies of three Laminaria species (Phaeophyceae)  
633 inhabiting different depth zones in the sublittoral region of Helgoland (North Sea) Mar.  
634 Ecol. Prog. Ser. 1: 195-207

635

636 Lüning, K. (1990). Seaweeds: their environment, biogeography, and ecophysiology.  
637 *John Wiley & Sons, New York, US*

638

639 Mcminn, A., Hirawake, T., Hamaoka, T., Hattori, H., and Fukuchi, M. (2005).  
640 Contribution of benthic microalgae to ice covered coastal ecosystems in northern  
641 Hokkaido, Japan. *Journal of the Marine Biological Association of the United Kingdom*,  
642 85(2):283–289.

643

644 MERIS Level 2 Detailed Processing Model.

645 [http://earth.esa.int/pub/ESA\\_DOC/ENVISAT/MERIS/MERIS\\_DPML2\\_i7r2A\\_re-](http://earth.esa.int/pub/ESA_DOC/ENVISAT/MERIS/MERIS_DPML2_i7r2A_re-issued.pdf)  
646 [issued.pdf](http://earth.esa.int/pub/ESA_DOC/ENVISAT/MERIS/MERIS_DPML2_i7r2A_re-issued.pdf)

647

648 Meleder, V., Populus J., Guillaumont, B., Perrot, T., Mouquet, P. (2010). Predictive

649 modelling of seabed habitats: case study of subtidal kelp forests on the coast of Brittany,  
650 France. *Marine Biology*, 157(7): 1525-1541

651

652 Morel, A. and Smith, R. C. (1974). Relation between total quanta and total energy for  
653 aquatic photosynthesis. *American Society of Limnology and Oceanography*, 19(4): 591–  
654 600.

655

656 Morel, A. (1988). Optical modeling of the upper ocean in relation to its biogenous  
657 matter content. *Journal of Geophysical Research*, 93:10749–10768.

658

659 Morel, A., Antoine, D., and Gentili, B. (2002). Bidirectional reflectance of oceanic  
660 waters: Accounting for Raman emission and varying particle phase function. *Applied Optic*,  
661 41: 6289–6306.

662

663 Morel, A., Huot, Y., Gentili, B., Werdell, P. J., Hooker, S. B. and Franz, B. A. (2007),  
664 Examining the consistency of products derived from various ocean color sensors in open  
665 ocean (Case 1) waters in the perspective of a multi-sensor approach. *Remote Sensing of*  
666 *Environnement*, 111: 69-88.

667

668 Mueller, J. L. (2000). SeaWiFS algorithm for the diffuse attenuation coefficient,  $K_{d490}$ ,  
669 using water-leaving radiances at 490 and 555 nm, *SeaWiFS Postlaunch Technical Report*  
670 *Series*, 24-27 pp, NASA Goddard Space Flight Center, Greenbelt, Maryland.

671

672 Pierson, D. C., Kratzer, S., Strombeck, N. and Hakansson B. (2008). Relationship  
673 between the attenuation of downwelling irradiance at 490 nm with the attenuation of PAR

674 (400 nm – 700 nm) in the Baltic Sea, *Remote Sensing of Environment*, 112: 668- 680.

675

676 Rasmus, K. E., Granbli, W., Wängberg, S.A. (2004). Optical studies in the Southern  
677 Ocean. *Deep-Sea Research*, 51: 2583-2597.

678

679 Rochford, P.A. , Kara, A.B. , Wallcraft, A.J., Arnone, R. A. (2001). Importance of solar  
680 subsurface heating in ocean general circulation models. *Journal of Geophysical Research*,  
681 106: 30923-30938.

682

683 Ryther, J. H. (1956). Photosynthesis in the ocean as a function of light intensity.  
684 *Limnology and Oceanography*, 1:61–70.

685

686 Sathyendranath, S. , Gouveia, A. D., Shetye, S. R., Ravindran, P. , Platt, T. (1991).  
687 Biological control of surface temperature in the Arabian Sea, *Nature*, 349:54-56.

688

689 Wang, M., Son, S., Harding, L. (2009). Retrieval of Diffuse Attenuation coefficient in  
690 the Chesapeake Bay and Turbid Ocean Regions for Satellite Ocean Color Applications.  
691 *Journal of geophysical research*, 114, c10011.

692

693 Wang, M., and W. Shi. (2005). Estimation of ocean contribution at the MODIS near-  
694 infrared wavelengths along the east coast of the U.S.: Two case studies, *Geophysical*  
695 *Research Letters*, 32, L13606.

696

697 Werdell, P.J. and Bailey S.W. (2005). An improved bio-optical data set for ocean color  
698 algorithm development and satellite data product validation. *Remote Sensing of*

699 *Environment*, 98(1):122-140.

700

701 Werdell, P.J. and BAILEY S.W. (2005), NASA Technical Memorandum 104566, vol 25

702

703 Zaneveld, J. R. V., Kitchen, J. C., AND Mueller J. L. (1993) Vertical structure of

704 productivity and its vertical integration as derived from remotely sensed observations,

705 *Limnology and oceanography*, 38: 1384-1393.

## 706 **VIII. Annex**

### 707 **A. Hydrolight / Ecolight settings**

708

709 Inherent optical properties

710 • Pure water absorption coefficient for 400-720nm from (Pope and Fry 1997)

711 • [Chl-a] constant with depth with values extracted from NOMAD.

712 • Default Hydrolight Chl-a absorption coefficient.

713 • Default Hydrolight Chl-a backscattering coefficient.

714 •  $A_{\text{cdm443}}$  from NOMAD.

715 • CDOM  $\gamma$  coefficient =  $-0.0176 \text{ nm}^{-1}$ .

716 • [SPM] from NOMAD and Eq. 14.

717 • Mineral particles specific scattering coefficient at 555nm =  $0.51 \text{ m}^2\text{g}^{-1}$

718 • Mineral particles specific absorption coefficient at 443nm =  $0.041 \text{ m}^2\text{g}^{-1}$

719 • Wavelengths similar to MERIS.

720 • Chlorophyll fluorescence effects not included

721

722 Geometry

723 • Solar zenith angle of  $40^\circ$

724 • Nadir viewing

725

726 Atmospheric and air-sea interface

727 • Surface wind speed of  $5 \text{ m s}^{-1}$

728 • Real index of refraction of water=1.34